The 2009 IEEE/RSJ International Conference on
Intelligent Robots and Systems
October 11-15, 2009 St. Louis, USA

Global Sliding Mode-Based Tracking Control of a Piezo-Driven XY Micropositioning Stage with Unmodeled Hysteresis

Qingsong Xu and Yangmin Li, *Senior Member, IEEE*

***Abstract*— In this paper, a global sliding mode control (GSMC) scheme is implemented on a piezo-driven XY parallel micropositioning stage to compensate for the unmodeled hysteresis aiming at a sub-micron accuracy motion tracking control. The GSMC controller is designed with the consideration of all uncertainty bounds. In the controller implementation, a high-gain velocity observer is adopted to estimate the feedback velocity from the measured position. The effectiveness of the GSMC over ordinary SMC and traditional PID control is demonstrated through simulations, while the variations of design parameters on control performances are examined as well. Results show that the GSMC can reduce the hysteresis to a negligible level and lead to a sub-micron accuracy tracking with tolerance to some degrees of external disturbances, which provides a sound base of practical control of the micropositioning system for micro/nano scale manipulation.**

I. INTRODUCTION

Micropositioning stages with piezoelectric actuation are applied more and more extensively in various ultra-precision applications [1]. Piezoelectric actuators (PZTs) are capable of nanometer resolution positioning with high stiffness and fast response, and hence usually employed to meet the requirements. Nevertheless, the major problem of piezo-driven stages comes from the nonlinearities introduced by PZT attributed to the hysteresis, creep, and drift effects. The hysteresis is reflected as the nonlinear relationship between the applied voltage and output displacement of PZT and induces a severe open-loop positioning error as high as 10–15% of the stage travel range. So, the hysteresis has to be suppressed for practical applications.

The successful compensation of hysteresis relies on the design of suitable control strategies. Typically, the hysteresis is compensated by the feedforward control resorting to an inverse hysteresis model based on the Preisach model and so on. Considering that most hysteresis models are only applicable with some particular input signal frequencies, a combined feedback control can be adopted for a precision motion control [2], [3]. For example, a sliding mode control with an inverse modified Prandtl-Ishlinskii model compensation is used in [4] for a precision positioning or tracking control. On the other hand, the establishment and identification of a hysteresis model is a complicated procedure leading to a time consuming work for a controller design process. Hence, more approaches without modeling the hysteresis have been exploited. To name a few, a traditional PI (proportional-integral) feedback controller is employed to compensate for the hysteresis in a nonopositioning stage [5], H_∞ robust controller designed with identified plant model [6] and inversion-based feedforward combined with polynomial-based feedback control [7] are implemented for high-bandwidth control of nanopositioning stages, respectively.

Actually, considering the hysteresis as a disturbance or uncertainty, sliding mode control (SMC) can be employed in a piezo-driven stage [8], since the major advantage of SMC lies in its robustness in the presence of model imperfection and uncertainties. SMC is a nonlinear control method which drives the nonlinear system's state trajectory onto a specified sliding surface and maintains the trajectory on this surface for the subsequent time. Since the control can be as simple as switching between two states, it is not sensitive to parameter variations and uncertainties entering into the control loop. Generally, a reaching phase motion exists in the conventional SMC before the system state arrives at the sliding surface. However, the existence of such a reaching phase reduces the robustness property of the control system [9]. In this research, a global sliding mode control (GSMC) strategy [10] eliminating the reaching phase is adopted to obtain a sliding mode during the entire system response. Specifically, a GSMC with the consideration of bounds on all uncertainties of the system is designed to compensate for the unmodeled hysteresis effects for an XY parallel micropositioning stage (PMS) [11]. Moreover, the advantages of GSMC over ordinary SMC for the motion tracking control will be demonstrated.

In the rest of the paper, after a brief description of the XY stage architecture and its dynamics uncertainties in Section II, an ordinary SMC and GSMC controllers are designed in Sections III and IV, respectively, and the stability of the closed-loop systems is proved via Lyapunov method. Based on the preliminary experimental test results in Section V, simulation studies are carried out in Section VI to verify the effectiveness of designed controllers. Particulary, the modified Prandtl-Ishlinskii model is used to represent the system with hysteresis, and a traditional PID controller is implemented as well for the purpose of comparison. Finally, some concluding remarks are summarized in Section VII.

II. SYSTEM DESCRIPTION AND DYNAMICS PROPERTY

A. Architecture Description of the XY Stage

As illustrated in Fig. 1, the XY parallel micropositioning stage (PMS) is designed with four identical PP (P stands

This work is supported by Macao Science and Technology Development Fund under Grant No.: 016/2008/A1 and the research committee of University of Macau under Grant No.: UL016/08-Y2/EME/LYM01/FST.

Q. Xu and Y. Li(corresponding author) are with the Department of Electromechanical Engineering, Faculty of Science and Technology, University of Macau, Av. Padre Tomás Pereira, Taipa, Macao SAR, P. R. China qsxu@umac.mo, ymli@umac.mo

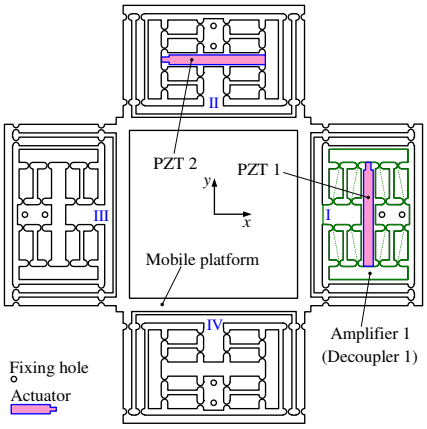

Fig. 1. A decoupled XY PMS.

for prismatic joint) limbs and actuated by two PZTs through the integrated displacement amplifiers. It is known that PZT can not bear transverse loads due to the risk of damage. The designed displacement amplifier acts as an ideal P joint and possesses larger ratio of stiffness in transverse direction than that in working direction. Hence, the amplifier also acts as a decoupler with the roles of transmitting axial force of actuator and preventing the actuator from suffering undesired transverse motions and loads as well. By this way, the two actuators are well isolated and protected. Moreover, the ideal translation provided by compound parallelogram flexures allows the generation of decoupled output motion for the stage. Different from a common decoupled XY PMS with output motion decoupling, the proposed one has both input and output decoupling in virtue of actuation isolation and decoupled output motion. This totally decoupling property is necessary for situations where the platform is under-actuated and sensory feedback of end-effector positions is not allowed. More details about the stage working principle can be found in [11].

B. Dynamic Model and Uncertainties

Since the stage is well decoupled, the two axial motions can be treated independently. Thus, two single-input-single-output (SISO) controllers can be employed for the X and Y axes, respectively. For conciseness, only the treatment of x-axis motion is presented in this paper.

Taking the micropositioning stage as a mass-spring-damper system, the dynamic model integrating the stage and PZT actuator can be derived as follows [12]:

$$M\ddot{x} + B\dot{x} + Kx = \frac{K_c T}{A_s(K_c + K_a)}(u - v), \qquad (1)$$

where the variable x denotes the x-axis displacement, M, B, and K represent the equivalent mass, damping parameter, and output stiffness of the system, respectively. Besides, K_c is input stiffness of the stage, K_a is stiffness of PZT actuator, A_s denotes the amplification ratio of output to input displacements of the stage, T is electromechanical transformer ratio of actuator, u represents input voltage applied to the actuator, and v denotes an internal voltage which induces hysteresis effects to the PZT.

It is observed that the left hand side of the model (1) represents a linear second order system, i.e.,

$$\ddot{x} + 2\xi\omega_n\dot{x} + \omega_n^2 x = \frac{K_c T}{A_s M(K_c + K_a)}(u - v), \qquad (2)$$

where ω_n is the natural frequency and ξ denotes the damping ratio of the stage system, which can be determined by experiments on open-loop transient response of the system.

As far as system parameters in (2) are concerned, actuator stiffness K_a is provided by the producer, the stiffness K_c and amplification ratio A_s can be determined by resorting to finite element analysis (FEA). Then the equivalent mass M can be derived accordingly. In addition, with a static signal input, the transformer ratio T of PZT can be derived by:

$$T = \frac{A_s M(K_c + K_a)\omega_n^2}{K_c}\frac{x}{u}, \qquad (3)$$

where the rate $\frac{x}{u}$ represents the slope of the rising or falling curves in displacement-voltage hysteresis loop, which is variable. Moreover, there exist uncertainties in the dynamic model since the aforementioned dynamic parameters can only be identified with some tolerances, and the complicated hysteresis can not be modeled accurately. To compensate for these uncertainties, a SMC can be employed since the major advantage of SMC lies in its robustness in existence of model imperfection and uncertainties. In the following sections, an ordinary sliding mode controller is constructed firstly.

III. ORDINARY SMC DESIGN

In this section, an ordinary SMC controller is designed to compensate for the unmodeled hysteresis, which is taken as a bounded disturbance v in (2).

The system model (2) can be rewritten into the form:

$$\ddot{x} + a\dot{x} + cx = b(u - v), \qquad (4)$$

where the nominal values for the variable parameters are

$$a = 2\xi\omega_n, \qquad (5)$$

$$c = \omega_n^2, \qquad (6)$$

$$b = \frac{K_c T}{A_s M(K_c + K_a)} > 0. \qquad (7)$$

Additionally, the error coordinates are defined as

$$e_1 = x - x_d, \qquad (8)$$

$$e_2 = \dot{x} - \dot{x}_d, \qquad (9)$$

where x_d denotes the desired position trajectory.

In view of the linear second order system, a sliding surface or switching function is selected as the first order function:

$$s = e_2 + \lambda e_1, \qquad (10)$$

where λ ($\lambda > 0$) is a design parameter. By taking the time derivative of both sides of (10), the following sliding dynamics can be obtained:

$$\begin{aligned}\dot{s} &= \dot{e}_2 + \lambda\dot{e}_1 \\ &= -(a - \lambda)\dot{x} - cx + b(u - v) - \ddot{x}_d - \dot{x}_d. \end{aligned} \qquad (11)$$

With the assignment of $\dot{s} = 0$ and $v = 0$, an equivalent control law for the reaching phase motion can be derived as:

$$u_{eq} = \frac{1}{b}\left[(a-\lambda)\dot{x} + cx + \ddot{x}_d + \lambda\dot{x}_d\right]. \tag{12}$$

In order to compensate for the uncertainty v, a corrective control law is designed below to guarantee the convergence of the state trajectory to the sliding surface:

$$u_c = -\beta \text{sign}(s) - \phi s, \tag{13}$$

where the switching gain β is selected as $\beta = \eta v_m$ with $\eta > 1$ so as to meet $\beta > v$ to guarantee the stability, ϕ is a positive constant to be designed, and the signum function sign(s) is:

$$\text{sign}(s) = \begin{cases} 1 & \text{for} \quad s > 0 \\ 0 & \text{for} \quad s = 0 \\ -1 & \text{for} \quad s < 0 \end{cases}. \tag{14}$$

As a summation of the two control items (12) and (13), the SMC control law is derived as:

$$u = u_{eq} + u_c. \tag{15}$$

To evaluate the stability, the following Lyapunov function candidate is considered:

$$V = \frac{1}{2}s^2. \tag{16}$$

Differentiating (16) with respect to time, results in

$$\dot{V} = s\dot{s}. \tag{17}$$

Substituting (11) into (17) with the consideration of (15), yields

$$\begin{aligned} \dot{V} &= -b[v + \eta v_m \text{sign}(s) + \phi s]s \\ &= -bvs - b\eta v_m|s| - b\phi s^2 \le 0. \end{aligned} \tag{18}$$

Thus, the sliding condition is satisfied by the designed control law (15). Furthermore, to alleviate the chattering phenomenon, the signum function in (15) is replaced by the saturation function with the notation:

$$\text{sat}(s) = \begin{cases} 1 & \text{for} \quad s > \delta \\ s/\delta & \text{for} \quad |s| \le \delta \\ -1 & \text{for} \quad s < -\delta \end{cases}, \tag{19}$$

where δ ($\delta > 0$) represents the boundary layer thickness.

A simulation study conducted shortly shows that the above SMC controller is not satisfactory for motion tracking control of the micropositioning system with complex hysteresis. Thus, an alternative SMC is designed in the subsequent section.

IV. GSMC DESIGN

In the GSMC, there exists no reaching phase motion, and a global sliding phase guarantees the robustness property of the controller. In what follows, a GSMC strategy with the consideration of all parameter uncertainties and unmodeled hysteresis is constructed for the micropositioning system.

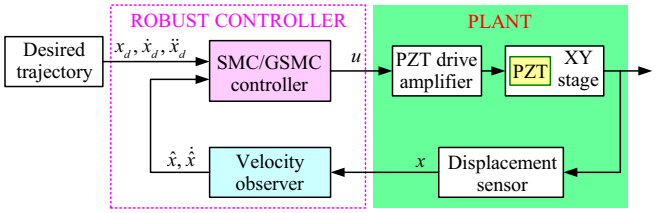

Fig. 2. Block diagram of the (global) sliding mode control.

A. GSMC Controller Design

In order to design a GSMC controller, it is assumed that the parameters in (4) are bounded by

$$b_{\min} \le b^{-1} \le b_{\max}, \tag{20}$$

$$a_{\min} \le ab^{-1} \le a_{\max}, \tag{21}$$

$$c_{\min} \le cb^{-1} \le c_{\max}, \tag{22}$$

$$v \le v_m. \tag{23}$$

Based on the error coordinates e_1 and e_2 defined in (8) and (9) with respective initial states e_{10} and e_{20}, a global sliding surface is selected as follows [10]:

$$s = e_2 + \lambda e_1 - f(t), \tag{24}$$

where the first order differentiable function $f(t) = f(0)e^{-kt}$ is designed to be $f(t) \to 0$ as $t \to 0$, with the initial value $f(0) = e_{20} + \lambda e_{10}$. It follows that the initial state locates in the sliding surface $s(0) = 0$, which means that the reaching phase is eliminated. Therefore, the global sliding mode can be obtained with the assigned sliding surface.

Taking the time derivative of both sides of (24), we have

$$\begin{aligned} \dot{s} &= \dot{e}_2 + \lambda\dot{e}_1 - \dot{f} \\ &= \ddot{x} - \ddot{x}_d + \lambda(\dot{x} - \dot{x}_d) - \dot{f} \\ &= \ddot{x} + (\lambda\dot{x} - \dot{f}) - (\ddot{x}_d + \lambda\dot{x}_d) \\ &= -a\dot{x} - cx + bu - bv + (\lambda\dot{x} - \dot{f}) - (\ddot{x}_d + \lambda\dot{x}_d). \end{aligned} \tag{25}$$

A global control with exponential asymptotic law is designed below:

$$\begin{aligned} u = &-\bar{b}(c\dot{x} - \dot{f}) + \bar{a}\dot{x} + \bar{c}x + \bar{b}(\ddot{x}_d + c\dot{x}_d) \\ &-\{\underline{b}|c\dot{x} - \dot{f}| + \underline{a}|\dot{x}| + \underline{c}|x| + v_m \\ &+\underline{b}|\ddot{x}_d + c\dot{x}_d|\}\text{sign}(s) - k|s|^r\text{sign}(s), \end{aligned} \tag{26}$$

where the design parameters $k > 0$, $0 < r < 1$, and

$$\bar{b} = \frac{b_{\max} + b_{\min}}{2}, \quad \underline{b} = \frac{b_{\max} - b_{\min}}{2}, \tag{27}$$

$$\bar{a} = \frac{a_{\max} + a_{\min}}{2}, \quad \underline{a} = \frac{a_{\max} - a_{\min}}{2}, \tag{28}$$

$$\bar{c} = \frac{c_{\max} + c_{\min}}{2}, \quad \underline{c} = \frac{c_{\max} - c_{\min}}{2}. \tag{29}$$

In order to prove the stability of the system, a Lyapunov function candidate is chosen as usual:

$$V = \frac{1}{2}s^2. \tag{30}$$

Substituting (26) into (25) and rearranging the items, gives an expression:

$$\begin{aligned} b^{-1}\dot{s} = &(b^{-1}-\bar{b})(\lambda\dot{x}-\dot{f}) - \underline{b}|\lambda\dot{x}-\dot{f}|\,\mathrm{sign}(s) \\ &-(b^{-1}-\bar{b})(\ddot{x}_d+\lambda\dot{x}_d) - \underline{b}|\ddot{x}_d+\lambda\dot{x}_d|\,\mathrm{sign}(s) \\ &+(\bar{a}-b^{-1}a)\dot{x} - \underline{a}|\dot{x}|\,\mathrm{sign}(s) \\ &+(\bar{c}-b^{-1}c)x - \underline{c}|x|\,\mathrm{sign}(s) \\ &-v - v_m\mathrm{sign}(s) - k|s|^r\mathrm{sign}(s). \end{aligned} \tag{31}$$

Differentiating (30) with respect to time, yields

$$\dot{V} = s\dot{s}. \tag{32}$$

Then, substituting (31) into (32) results in

$$\begin{aligned} b^{-1}\dot{V} = &b^{-1}s\dot{s} \\ = &(b^{-1}-\bar{b})(\lambda\dot{x}-\dot{f})s - \underline{b}|\lambda\dot{x}-\dot{f}||s| \\ &-(b^{-1}-\bar{b})(\ddot{x}_d+\lambda\dot{x}_d)s - \underline{b}|\ddot{x}_d+\lambda\dot{x}_d||s| \\ &+(\bar{a}-b^{-1}a)\dot{x}s - \underline{a}|\dot{x}||s| - vs - v_m|s| \\ &+(\bar{c}-b^{-1}c)xs - \underline{c}|x||s| - k|s|^{r+1}. \end{aligned} \tag{33}$$

In view of (20)—(22), we can derive that

$$b^{-1}-\bar{b} \le \underline{b}\,, \tag{34}$$

$$\bar{a}-b^{-1}a \le \underline{a}\,, \tag{35}$$

$$\bar{c}-b^{-1}c \le \underline{c}\,. \tag{36}$$

Finally, substituting the above (34)—(36) into (33) and considering (7) and (23), we can deduce that

$$\dot{V} \le 0, \tag{37}$$

which means that the closed-loop system is stable.

Furthermore, to alleviate the chattering phenomenon, the signum function in control law (26) is replaced by the saturation function described in (19) as well.

B. Controller Implementation

An insight into (26) and (15) indicates that both full state feedback and full state trajectory are required to implement the GSMC or SMC controller. Although the full state trajectory can be generated by differentiating the desired position trajectory in advance, the velocity feedback has to be estimated since only the position can be measured by the displacement sensor. Generally, the velocity can be estimated by resorting to the measured position using a backward difference equation:

$$\dot{x} = \frac{x(t_i)-x(t_{i-1})}{t_s}, \tag{38}$$

where $x(t_i)$ denotes the measured position at the i-th sampling time t_s. In spite of its simplicity, it has limitations due to the accuracy and quantization noise, which restricts the achievable bandwidth of the feedback controller. Alternatively, a closed-loop high-gain observer can be employed without the above limitations [13]. Thus, a high-gain observer is adopted to estimate the feedback velocity as follows:

$$\begin{bmatrix}\dot{y}_1\\ \dot{y}_2\end{bmatrix} = \begin{bmatrix}-\beta_1/\tau & 1\\ -\beta_2/\tau^2 & 0\end{bmatrix}\begin{bmatrix}y_1\\ y_2\end{bmatrix} + \begin{bmatrix}\beta_1/\tau\\ \beta_2/\tau^2\end{bmatrix}x, \tag{39}$$

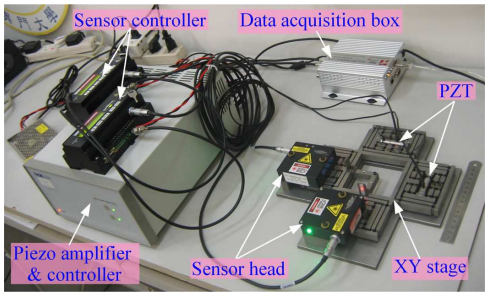

Fig. 3. Photograph of experimental setup.

where the measured x is the position input to the observer, and the observer output is the full state feedback, i.e., $\hat{x} = y_1$ and $\dot{\hat{x}} = y_2$. The bandwidth of the observer depends on design gains β_1 and β_2, and the accuracy of the estimated velocity relies on the design parameter τ.

Therefore, the robust controller is constructed by the above two components of GSMC (or SMC) controller and velocity observer. The block diagram of the control scheme is illustrated in Fig. 2. It can be observed that the input to the robust controller is the desired position, velocity, and acceleration trajectories and measured position, while the output is the voltage that will be applied to drive the PZT.

V. HARDWARE CONFIGURATION AND PRELIMINARY TEST

The experimental setup of the XY stage prototype is graphically shown in Fig. 3. The monolithic stage is fabricated from a piece of light material Al 7075-T651. Two 20 μm-stroke PZT (model PAS020 produced by Thorlabs, Inc.) are adopted to drive the XY stage, and the PZT is actuated with a voltage of 0–75 V through a two-axis piezo amplifier and controller (BPC002 from the Thorlabs). The displacements of the output mobile platform are measured by two laser displacement sensors (Microtrak II, head model: LTC-025-02, from MTI Instrument, Inc.). The analog voltage outputs of the two sensors are connected to a three-channel data acquisition box (UBOX-20016 from TDEC Ltd.), which is embedded with 16-bit A/D convertors. The digital output of the acquisition box is then simultaneously read by a personal computer through a USB interface. The resolution of the displacement detecting system is 0.04 μm.

Preliminary open-loop test shows that the XY stage has a workspace around 120 μm$\times$120 μm with the maximum cross-talk of 1.5% between the two axes, which verifies the well-decoupled property. From open-loop step response test, the damping ratio $\xi = 0.12$ and natural frequency $\omega_n = 1054.9$ rad/s can be identified. Besides, for the developed XY micropositioning stage, the amplification ratio $A_s = 6.2$, output stiffness $K = 1.84 \times 10^5$ N/m, and input stiffness $K_c = 9.9 \times 10^6$ N/m can be obtained by FEA simulation. So, the equivalent mass and damping parameter can be determined as $M = 0.165$ kg and $B = 41.86$ N·s/m, respectively. Besides, the actuator's stiffness $K_a = 5 \times 10^7$ N/m is provided by the manufacturer, and the $\bar{T} = 10.85$ C/m is the nominal value for the transformer ratio. After that,

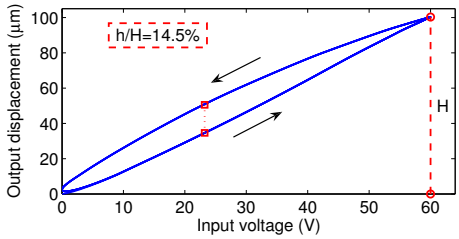

Fig. 4. Open-loop hysteresis loop of the micropositioning system produced by the identified modified Prandtl-Ishlinskii hysteresis model with a 0.125-Hz input rate.

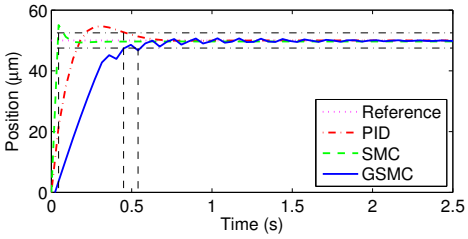

Fig. 5. Comparison of 50-μm step response test results with different control method.

nominal values for a, b, and c in (4) can then be calculated according to (5)—(7). The effectiveness of the designed controller is demonstrated in the subsequent discussions.

VI. SIMULATION STUDIES AND RESULTS

A. Controller Setup

In the current research stage, numerical simulations are performed with MATLAB to discover the efficiencies of the design GSMC as well as ordinary SMC controller. Besides, an incremental type PID controller is also implemented for the comparison purpose. The gains of the PID control are tuned to maintain the overshoot within 10%, i.e., $K_P = 0.91$, $K_I = 0.37$, and $K_D = 0.06$.

In the simulation, the plant as indicated in Fig. 2 is expressed by the modified Prandtl-Ishlinskii hysteresis model [14], which is identified based on experimental data provided by the laser displacement sensor with an input signal rate of 0.125 Hz. For a periodical sinusoidal wave voltage input covering the voltage range of 0 to 60 V, the hysteresis loop produced by the identified modified Prandtl-Ishlinskii model is shown in Fig. 4.

It is observed that the hysteresis leads to certain differences between the rising and falling displacement-voltage curves. Concretely, the maximum width of the hysteresis loop is as high as 14.5% of the travel range, which provides a challenge for the controller design. Additionally, it is seen that $v_m = 9.5$ V, which is the maximum difference in input voltage between the rising and falling curves with respect to the same output displacement value. The uncertain ratio T is bounded within $0.9\bar{T} \leq T \leq 1.1\bar{T}$. Thus, the uncertainty bounds for parameters b, a, and c can be calculated by (20)—(22). Additionally, the sampling time interval is assigned as $t_s = 0.045$ s to simulate the real situation achievable with the current hardware. Besides, $\lambda = 9800$, $\eta = 5$, $\phi = 450$, and $\delta = 10$ are assigned for the ordinary SMC and $\lambda = 18$, $k = 0.5$, $r = 0.5$, and $\delta = 50$ are chosen for the GSMC, respectively.

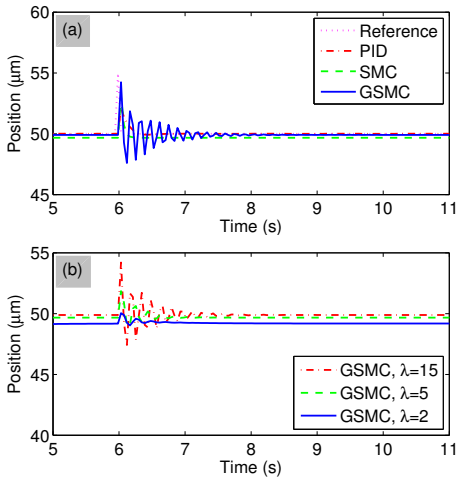

Fig. 6. Comparison of step responses with external disturbance. (a) Responses of the three controllers, (b) response of the GSMC with different λ values.

B. Control Results and Discussions

First, the step responses for a 50-μm displacement input are tested and the results are plotted in Fig. 5. The controller parameters are tuned to obtain a response as rapid as possible within 10% overshoot magnitude. It is observed that the settling time (with 5% tolerance) for the three controllers are: $t_{SMC} < t_{PID} < t_{GSMC}$. That is, the SMC produces the most rapid transient response among the three controllers, while GSMC can only creates the lowest response speed. Moreover, it is found that as the increasing of control parameters λ for SMC and GSMC controllers, quicker responses with smaller steady-state errors can be obtained which are at the expense of higher overshoot and clearer chattering, respectively.

In addition, to test the robustness property of the three controllers for disturbances rejection, the input signal is increased by a factor of 10% at the time of 6 s. The control results are compared in Fig. 6(a). It can be seen that all of the controllers can tolerate the disturbances since the control results return to the normal values quickly, except for a larger oscillation in the GSMC response. The tuning of control parameters shows that the oscillation magnitude can be reduced by decreasing the value of λ for GSMC as illustrated in Fig. 6(b). As can be expected, the decreasing of λ results in a slower initial response and a larger steady-state error on the other hand. Hence, a tradeoff between the performances is necessary to select the control parameters for practical applications.

Besides, a 0.125-Hz 60-μm sinusoidal motion tracking control is performed by employing the three controllers and the results are described in Fig. 7. We can observe that the GSMC is superior to both PID and SMC controllers in terms of peak-to-peak (p-p) tracking error. In addition, the SMC is not superior to PID since the p-p error is only reduced from

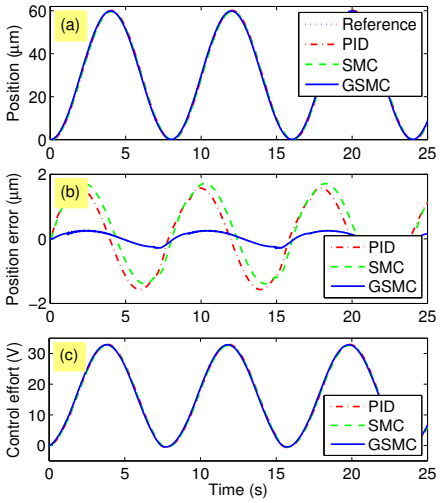

Fig. 7. 0.125-Hz sinusoidal motion tracking. (a) Tracking result, (b) tracking error, (c) control effort.

3.14 μm to 3.10 μm by SMC as indicated in Fig. 7(b). In contrast, with the GSMC, the p-p error has been significantly reduced to 0.56 μm. This is the main reason why GSMC is designed although SMC is implemented at first. Additionally, from the controller output signal as shown in Fig. 7(c), we can see that no chattering exists in the control signal. Based on the designed controllers, the hysteresis of the system is tested as well. For the travel range of 100 μm, the hysteresis loop is reduced to 3.4%, 2.9%, and 0.4% by PID, SMC, and GSMC controllers, respectively. Therefore, the GSMC substantially reduces the hysteresis to a negligible level.

Moreover, as the increasing of input rate from 0.0625 to 0.5 Hz, the corresponding tracking control has been conducted and percentage p-p errors with respect to the travel range are summarized in Fig. 8. As can be observed that the control errors increase correspondingly as the rising of input rate due to the bandwidth capability of the implemented controllers. The best performance of GSMC over PID and SMC is clear to see. With the GSMC method, to maintain the p-p error within 6% of the tracking range, the input rate should be restricted within 0.5 Hz.

In summary, among the three implemented controllers, SMC is more proper to set-point regulation while GSMC is more suitable for motion tracking control of the developed XY micropositioning system. It is noticeable that the bandwidth of a feedback controller relies on the sampling frequency heavily. In order to reduce the control error with higher input rate, one immediate future work is to implement a shorter sampling time, which depends on the data acquisition hardware available. Besides, experimental studies with the designed controller will be conduced as well for practical applications in our future works.

VII. CONCLUSION

The major contribution of this paper lies in the design of a suitable controller for an XY parallel micropositioning stage to compensate for the unmodeled hysteresis effects. It is verified that the dominate hysteresis phenomenon can

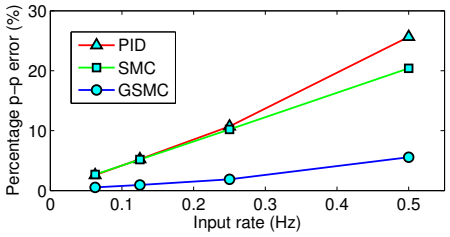

Fig. 8. Percentage peak-to-peak error versus input rate.

be suppressed by employing a GSMC approach. The performances of the implemented GSMC over PID and SMC controllers have been illustrated by extensive simulation studies. Results show that the hysteresis can be reduced to a negligible level of 0.4% with the GSMC controller, and the peak-to-peak tracking error is maintained within 6% of the overall travel range with an input rate lower than 0.5 Hz. In our future works, high-rate tracking control will be implemented and tested on the prototype for real micro/nano scale manipulation, which heavily depends on the hardware available.

REFERENCES

[1] J. J. Abbott, Z. Nagy, F. Beyeler, and B. J. Nelson, "Robotics in the small, part I: Microrobotics," *IEEE Robot. Automat. Mag.*, vol. 14, no. 2, pp. 92–103, 2007.

[2] G. Song, J. Zhao, X. Zhou, and J. De Abreu-Garcia, "Tracking control of a piezoceramic actuator with hysteresis compensation using inverse Preisach model," *IEEE/ASME Trans. Mechatron.*, vol. 10, no. 2, pp. 198–209, 2005.

[3] C.-J. Lin and S.-R. Yang, "Precise positioning of piezo-actuated stages using hysteresis-observer based control," *Mechatronics*, vol. 16, no. 7, pp. 417–426, 2006.

[4] J.-C. Shen, W.-Y. Jywe, H.-K. Chiang, and Y.-L. Shu, "Precision tracking control of a piezoelectric-actuated system," *Precis. Eng.*, vol. 32, no. 2, pp. 71–78, 2008.

[5] H. G. Xu, T. Ono, and M. Esashi, "Precise motion control of a nanopositioning PZT microstage using integrated capacitive displacement sensors," *J. Micromech. Microeng.*, vol. 16, no. 12, pp. 2747–2754, 2006.

[6] S. Salapaka, A. Sebastian, J. P. Cleveland, and M. V. Salapaka, "High bandwidth nano-positioner: A robust control approach," *Rev. Sci. Instrum.*, vol. 73, no. 9, pp. 3232–3241, 2002.

[7] S. S. Aphale, S. Devasia, and S. O. R. Moheimani, "High-bandwidth control of a piezoelectric nanopositioning stage in the presence of plant uncertainties," *Nanotechnology*, vol. 19, p. 125503, 2008.

[8] H. C. Liaw, B. Shirinzadeh, and J. Smith, "Robust motion tracking control of piezo-driven flexure-based four-bar mechanism for micro/nano manipulation," *Mechatronics*, vol. 18, no. 2, pp. 111–120, 2008.

[9] T. L. Tai and Y. S. Lu, "Global sliding mode control with chatter alleviation for robust eigenvalue assignment," *Proc. IMechE Part I: J. Systems and Control Engineering*, vol. 220, no. 7, pp. 573–584, 2006.

[10] J. Liu, *MATLAB Simulation for Sliding Mode Control*. Beijing: Tsinghua University Press, 2005.

[11] Y. Li and Q. Xu, "Design and analysis of a totally decoupled flexure-based XY parallel micromanipulator," *IEEE Trans. Robot.*, vol. 25, no. 3, pp. 645–657, 2009.

[12] J. J. Gorman and N. G. Dagalakis, "Modeling and disturbance rejection control of a nanopositioner with application to beam steering," in *Proc. of ASME Int. Mechanical Engineering Congress and Exposition*, 2003, IMECE2003-41603.

[13] S.-M. Yang and S.-J. Ke, "Performance evaluation of a velocity observer for accurate velocity estimation of servo motor drives," *IEEE Trans. Ind. Applicat.*, vol. 36, no. 1, pp. 98–104, 2000.

[14] K. Kuhnen, "Modeling, identification and compensation of complex hysteretic nonlinearities: A modified Prandtl-Ishlinskii approach," *European J. Control*, vol. 9, no. 4, pp. 407–421, 2003.